ACS APPLIED MATERIALS & INTERFACES

Research Article

www.acsami.org

Selective SERS Detecting of Hydrophobic Microorganisms by Tricomponent Nanohybrids of Silver−Silicate-Platelet−Surfactant

Jun-Ying Ho,[†] Ting-Yu Liu,*[,†,‡] Jiun-Chiou Wei,[†] Juen-Kai Wang,[§,∥] Yuh-Lin Wang,[∥,⊥] and Jiang-Jen Lin*[,†]

[†]Institute of Polymer Science and Engineering, National Taiwan University, Taipei 10617, Taiwan

[‡]Department of Materials Engineering, Ming Chi University of Technology, New Taipei City 24301, Taiwan

[§]Center for Condensed Matter Sciences, National Taiwan University, Taipei 10617, Taiwan

[∥]Institute of Atomic and Molecular Sciences, Academia Sinica, Taipei 10617, Taiwan

[⊥]Department of Physics, National Taiwan University, Taipei 10617, Taiwan

Supporting Information

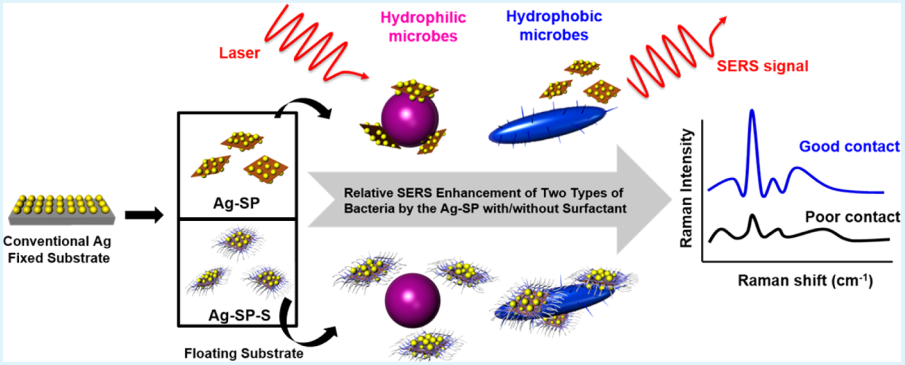

ABSTRACT: Nanohybrids consisting of silver nanoparticles (Ag), clay platelets, and a nonionic surfactant were prepared and used as the substrate for surface-enhanced Raman scattering (SERS). The nanoscale silicate platelets (SP) (with dimensions of 100 × 100 nm^2 and a thickness of ∼1 nm) were previously prepared from exfoliation of the natural layered silicates. The tricomponent nanohybrids, Ag-SP-surfactant (Ag-SP-S), were prepared by in situ reduction of $AgNO_3$ in the presence of clay and the surfactant. The clay platelets with a large surface area and ionic charge (ca. 18 000 sodium ions per platelet) allowed for the stabilization of Ag nanoparticles in the range of 10−30 nm in diameter. With the addition of a nonionic surfactant such as poly(oxyethylene) alkyl ether, the tricomponent Ag-SP-S nanohybrids possessed an altered affinity for contacting microorganisms. The particle size and interparticle gaps between neighboring Ag on SP were characterized by TEM. The surface tension of Ag-SP and Ag-SP-S in water implied different interactions between Ag and hydrophobic bacteria (*Escherichia coli* and *Mycobacterium smegmatis*). By increasing the surfactant content in Ag-SP-S, the SERS peak intensity was dramatically enhanced compared to the Ag-SP counterpart. The nanohybrids, Ag-SP and Ag-SP-S, with the advantages of varying hydrophobic affinity, floating in medium, and 3D hot-junction enhancement could be tailored for use as SERS substrates. The selective detection of hydrophobic microorganisms and larger biological cells makes SERS a possible rapid, label-free, and culture-free method of biodetection.

KEYWORDS: *surface-enhanced Raman scattering, silver nanoparticle, silicate platelet, surfactant*

1. INTRODUCTION

New developments in metal nanoparticles and organic/inorganic nanocomposites have advanced nanotechnology over the past decade. In particular, biosensor technology[1,2] has made great progress through the invention of noble-metal nanostructured materials. For example, traditional methods of detecting pathogens involve the basic steps of pre-enrichment, selective enrichment, biochemical screening, and serological confirmation.[3−7] Each step is a selective and specific process that often requires tedious procedures and a fast remedial response.[8] Thus, it is desirable to have highly sensitive, selective, and efficient diagnostic systems, such as surface-enhanced Raman spectroscopy (SERS). This powerful analytical tool enables the identification and detection of microorganisms in a direct manner because of its unique vibrational signatures associated with chemical and structural information.[9−17]

Received: September 26, 2013
Accepted: January 10, 2014
Published: January 10, 2014

Scheme 1. Three Different Fabrication Processes Routes from Nanoscale Silicate Platelets, SP, Prepared from the Exfoliation of Na^+-MMT[a]

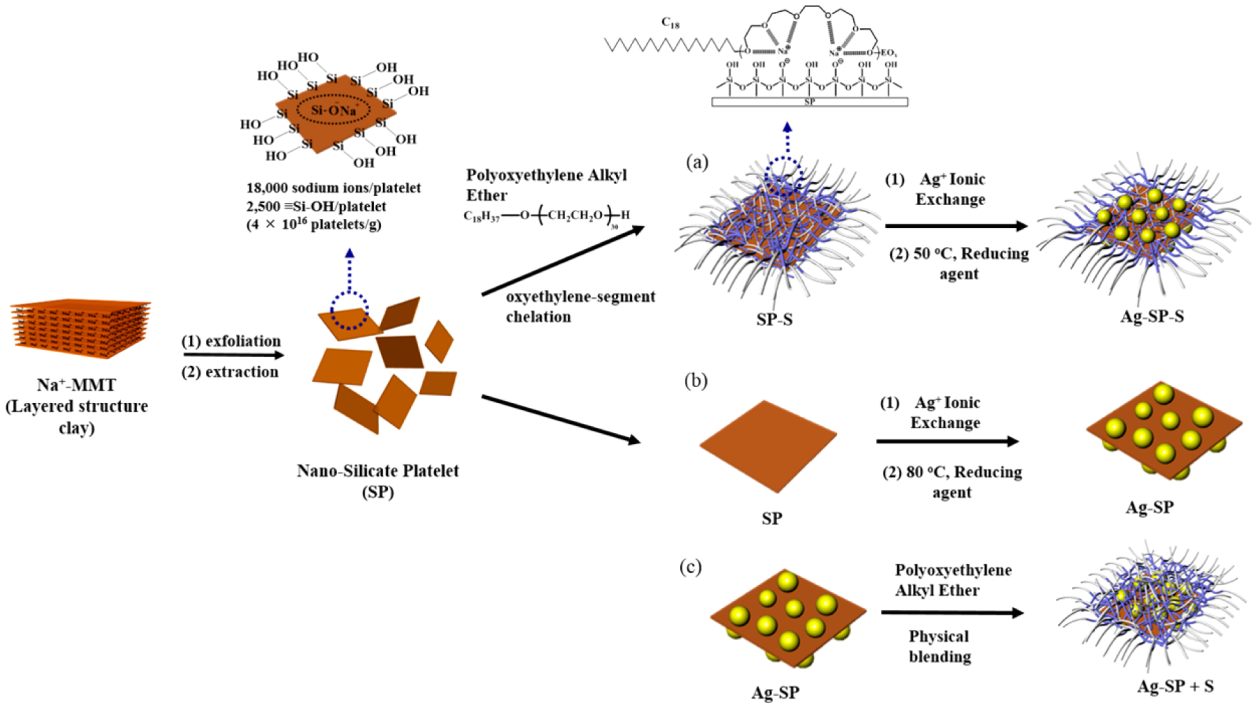

[a](a) Ag-SP-S preparation from in situ reduction of $AgNO_3$ in the presence of surfactant and SP; (b) Ag-SP by in situ reduction of $AgNO_3$ and SP without surfactant; and (c) Ag-SP+S preparation from physical blending the reduced Ag-SP and a surfactant.

In our previous works, metal nanoparticles and clay hybrids were synthesized for diverse applications in electronics,[18,19] oil recovery,[20] and biomedical applications such as bacterial growth inhibition[21−26] and wound healing.[27] Silicate platelets (SP) with dimensions of 100 × 100 × 1 nm^3 were prepared from exfoliation of natural silicate clays[19,28] such as sodium montmorillonite (Na^+-MMT). Because of the nanometer-thickness, high-surface area, and multiple negative charges on the surface,[29] the SP was found to have antimicrobial properties but with less cell endocytosis or genotoxicity.[30] As the support, the SP could stabilize Ag nanoparticles from aggregation and generate different compositions of Ag-SP bicomponent hybrids. The nanoscale-thin platelets have an increased affinity for contacting microorganisms through surface polar interactions. It is anticipated that this class of Ag nanohybrids might demonstrate enhanced performance if using as SERS substrates[28] for detecting microbes because the Ag was regularly tethered on the platelet surface. Furthermore, it is known that the Ag nanostructure exhibits strong surface plasmons across the spectrum from 300 to 1200 nm in the visible and near-infrared regions.[29] The Ag nanoparticles on both sides of the 1 nm thick SP may allow for the generation of strong localized surface plasma resonance (LSPR) in the $x-y$ directions and particularly in the z direction of individual platelets, termed 3D hot junctions.[10,14,30]

Here, we report a new class of tricomponent nanohybrids by an in situ process of surfactant modification onto Ag-SP with different compositions and varied selectivity for contacting hydrophobic bacteria. The newly developed SERS substrate (Ag-SP-S) has varied surface activities and interacts differently toward hydrophobic and hydrophilic microbes. With a suitable selection of nonionic surfactant, the nanohybrids, Ag-SP-S, significantly changed their surface tension when used as the SERS substrate in contact with microbes. Hence, the tricomponent nanohybrids consisting of surfactant-modified silicate platelet (SP-S) and tethered Ag nanoparticles could render the selective detection of hydrophobic microbes. Owing to the presence of ionic species (≡Si−O^-Na^+) on the surface, the SP displayed a hydrophilic nature that could be altered by surfactant modification. Consequently, the SP may enhance the ability of the Ag nanoparticles to contact the microbial surface, thereby increasing SERS sensitivity. Recent research efforts have focused on the design of high-performance SERS-active substrates for detecting particular molecules,[31−37] but there has been less focus on utilizing this approach for large microorganisms such as bacteria, fungi, and mycobacterium. The SERS-enhancing behavior that takes place between a substrate in contact with a large microbial entity is still not well understood. For the purpose of pathogen detection, the development of a tricomponent nanohybrids system may lead to the improvement of detection sensitivity over conventional SERS substrates. Overall, the introduction of a nonionic surfactant adjusts the surface energy of Ag-SP to facilitate intimate contacts with a variety of organisms and particularly tailors the affinity towards hydrophobic microbes.

The selection of a polymer or ionic surfactant has been reported for adjusting the surface energy of nanomaterials, enabling high selectivity for microbes.[38−41] In general, cationic surfactants such as dodecyltrimethyl ammonium bromide (DDTMA) can perform an ionic-exchange reaction between alkyl quaternary ammonium salts and sodium ions in the SP clay surface, but this leads to a lipophilic surface that does not stabilize Ag. However, anionic surfactants such as sodium dodecyl sulfate (SDS) are not able to interact well with SP through the ionic-exchange reaction. Hence, nonionic surfactants such as alkyl alcohol ethoxylates or poly-

(oxyethylene) alkyl ether oligomers are suitable for associating SP by dipole−dipole interactions.[42] By judiciously selecting the nonionic surfactant, we prepared Ag-SP-S by in situ reduction of $AgNO_3$ in the presence of SP and surfactant in water. In comparison with conventional SERS of the fixed Ag nanoparticle substrate, the prepared Ag-SP-S may serve as floating substrates in medium for selectively detecting hydrophilic microbes such as *Staphylococcus aureus* as well as hydrophobic microbes such as *Escherichia coli* and *Mycobacterium smegmatis*, depending on the species of the surfactants. More specifically, we report the preparation of the surfactant-modified Ag-SP tricomponent nanohybrids as the floating substrate to achieve high-performance SERS sensitivity and the selectivity of sensing hydrophobic or hydrophilic bacteria.

2. EXPERIMENTAL SECTION

Nanoscale silicate platelets (SP) were previously prepared by exfoliating the Na^+ form of layered silicate clay, montmorillonite (Na^+-MMT, Nanocor Co.).[43] Na^+-MMT is a natural smectite aluminosilicate that has a generic structure of 2:1 layered silicate to aluminum oxides with two tetrahedral sheets sandwiching an edge-shared octahedral sheet and exchangeable Na^+ counterions with a CEC of 120 mequiv/100 g. The process of exfoliation involved using polymeric amine salts for the ionic-exchange reaction and subsequent extraction into a water slurry.[43] The isolated silicate platelets are nearly 1 nm in thickness and ca. 100 × 100 nm^2 in lateral dimensions. Detailed characterizations of the ionic charges were previously reported.[19] The exfoliated SP was then used as the support for generating Ag nanoparticles on SP nanohybrids. Silver nitrate ($AgNO_3$, M_w = 169.8 g/mol, J. T. Baker, Inc.) was used as the silver precursor. Ethanol (99.9%, Aldrich) was utilized as the weak reducing agent and solvent. Diethanolamine (>98%, Aldrich) was additionally utilized as a reducing agent for reducing $AgNO_3$. Nonionic surfactant, poly(oxyethylene) C18-alkyl ether (SINOPOL 1830), was obtained from Sino-Japan Chemical Co. All aqueous solutions were prepared with deionized water. Bacterial strains, including Gram-negative *E. coli* (DH5α) and Gram-positive *S. aureus* were obtained from Super Laboratory Co. (Taiwan). *M. smegmatis* (ATCC 609) cells were obtained from American Type Culture Collection (ATCC).

2.1. Synthesis of Ag-SP-S Nanohybrids by an in Situ Chemical Process. The procedure for the in situ synthesis of the Ag-SP-S nanohybrids is as follows (Scheme 1a). Poly(oxyethylene) C18-alkyl ether (SINOPOL 1830) was added into silicate platelets in slurries. An aliquot of 1 wt % SP in a water suspension (25 g) was added to 1 wt % SINOPOL 1830 in a water suspension (25g) in a round-bottomed flask equipped with mechanical stirrer bar, and the mixture was stirred for 30 min at room temperature. The SP-S solution (50 g, 1 wt % in water) was added to the $AgNO_3$ solution (33.7 g, 1 wt % in water) and mechanically stirred for 10 min at room temperature. To prevent the possible formation of silver oxide, nitrogen was introduced to fill the reactor. The conversion involved the replacement of Ag^+ for Na^+ counterions on the SP clay surface and, consequently, the reduction of Ag^+ to Ag^0 by diethanolamine (4.2 g, 10 wt % in water). The reaction mixture was then slowly heated to 50 °C and maintained for 20 h under continuous agitation. During the process, the mixture was monitored by UV-vis spectroscopy for the color change from yellow to deep-red, indicating the reduction of Ag^+ to Ag^0. In this study, we prepared eight samples of Ag-SP-S with different surfactant compositions (i.e., 30/70/8, 30/70/17, 30/70/35, and 30/70/70 as well as another series, 30/35/8, 30/35/17, 30/35/35, and 30/35/70 (w/w/w), with a higher silver component for comparison).

2.2. Synthesis of Ag-SP+S by Physical Blending. We attempted the synthesis by physical blending of the Ag-SP nanohybrids and surfactant (Ag-SP+S), as described in Scheme 1c. In other words, the Ag-SP was first prepared by silver nitrate reduction in the presence of SP (Scheme 1b) and then mixed with SINOPOL 1830 surfactant under physical stirring for 30 min. The example of preparing Ag-SP+S (30/70+70) is described. An aliquot of SP solution (7.59 g, 9.22 wt % in water) was dispersed in deionized water (19.46 g) followed by the addition of ethanol (49.5 g) and mechanical stirring for 30 min. Then, $AgNO_3$ (23.62 g, 2 wt % in water) was added, and stirring was continued for 30 min. The Ag-SP (30/70) solutions were filtered, washed with ethanol, and redissolved in water. The UV absorption at ∼400 nm of the final solution indicated the formation of Ag nanoparticles. Finally, the nonionic surfactant SINOPOL 1830 (0.29 g, 4 wt %) was added to the Ag-SP slurries (2 g, 0.84 wt %), and the mixture was stirred for 30 min at room temperature to obtain the physically blended hybrids .

By using similar procedures, we prepared 14 samples of Ag-SP+S (i.e. 30/70+10, 30/70+20, 30/70+30, 30/70+40, 30/70+50, 30/70+60, and 30/70+70 as well as another series, 7/93+10, 7/93+20, 7/93+30, 7/93+40, 7/93+50, 7/93+60, and 7/93+70). The comparison of nanohybrids prepared from the physical blending and in situ reduction procedures was investigated to differentiate the surfactant effects of Ag-SP+S from the in situ synthesized Ag-SP-S.

2.3. Bacteria Growth and Sample Preparation. *S. aureus* and *E. coli* were cultivated for 16 h at 37 °C on LB agar base. After subculturing, single colonies were collected using sterile plastic inoculating loops. Bacteria were then suspended in 5 mL of LB broth, grown for an additional 18 h, and then subcultured until OD_{600} reached approximately 0.5. *M. smegmatis* cells were cultivated for 48 h at 37 °C on L-J agar slant base (Creative Microbiologicals, Ltd.). After subculturing, single colonies were collected using sterile plastic inoculating loops. Bacteria were then suspended in 5 mL of Middlebrook 7H9 broth medium (Creative Microbiologicals, Ltd.) and grown for another 48 h at 37 °C. Before SERS detection, bacteria were washed, centrifuged three times with deionized water, and resuspended in water again. The washed bacteria solution (100 μL, 10^8 CFU/mL of bacteria) was mixed with 100 μL of the Ag nanohybrids solution ([Ag] = 100 ppm) and dropped onto a glass-based aluminum chip. Typically, the sample solution (1.0 mL) was placed on a SERS substrate and then stored in an orbital shaking incubator (OSI500R, TKS) operated at 120 rpm and 37 °C for 1 h.

2.4. Characterization. Raman spectra were collected with a commercial Raman microscope (HR800, Horiba). A He−Ne laser emitting at 632.8 nm was used as the excitation source, and the laser beam was focused onto the sample through a 50× objective lens. The backward radiation was collected by the same lens and delivered to an 80 cm spectrograph equipped with a liquid-nitrogen cooled charge-coupled device for spectral analysis. Raman spectra were collected in the frequency range from 400 to 1800 cm^{-1} with a typical acquisition time of 30 sec. A background subtraction and spectrum average program, based on the algorithm proposed by M. Miroslav's group,[44] was developed to process the obtained Raman spectra. Each SERS spectrum was measured at with least six repetitions (n > 6) and the SERS peaks were averaged. The diameter (d) of Ag nanoparticles was measured by examining transmission electron microscopy (TEM, JOEL JEM-1230) images and by counting using commercial software (Scanning Probe Image Processor, SPIP). The interaction between nanohybrids (Ag-SP and Ag-SP-S) and bacteria (*E. coli* and *S. aureus*) was imaged by field-emission scanning electronic microscopy (FE-SEM, JEOL-6500) at an accelerating voltage of 15 kV. X-ray powder diffraction (XRD) was used to characterize the Ag nanoparticles by using a Shimadzu SD-D1 with Cu Kα radiation (35 kV, 30 mA). X-ray photoelectron spectroscopy (XPS, VG Scientific ESCALAB 250, UK) of Si 2p and O 1s electrons revealed information on the Ag−Si interaction. The surface tension of Ag-SP and Ag-SP-S in solution (∼1 wt % range) was measured by the Wilhelmy method using a Kruss-K10 digital tensiometer equipped with a spherical ring.

3. RESULTS AND DISCUSSION

Two synthetic methods to produce the nanohybrids of nanosilicate platelets (SP) and Ag nanoparticles are conceptually illustrated in Scheme 1. The SP was prepared previously from the exfoliation of natural clay (Na^+-MMT) with a layered structure. The in situ reduction of $AgNO_3$ to generate Ag nanoparticles (Ag) in the presence of SP and surfactant

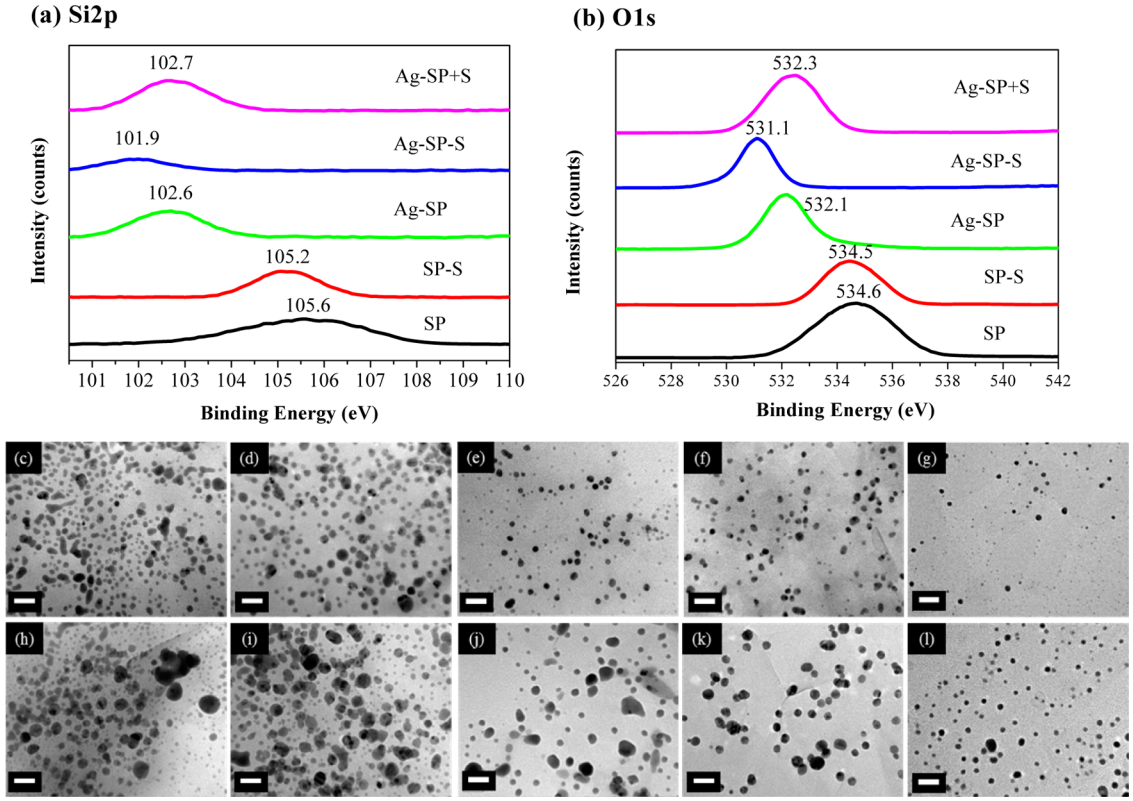

Figure 1. XPS spectra of SP, SP-S silicate supports, and silver nanoparticle compounds Ag-SP, Ag-SP-S, and Ag-SP+S for (a) Si 2p and (b) O 1s spectroscopy. TEM images of in situ synthesis of (c–g) Ag-SP-S 30/70 with various surfactant ratios from 0 to 70: (c) 30/70/0, (d) 30/70/8, (e) 30/70/17, (f) 30/70/35, and (g) 30/70/70; (h–l) Ag-SP-S 30/35 with various surfactant ratios from 0 to 70: (h) 30/35/0, (i) 30/35/8, (j) 30/35/17, (k) 30/35/35, and (l) 30/35/70. (The scale bar is 50 nm.)

afforded Ag-SP-S (Scheme 1a). The physically blended Ag-SP+S was obtained by making Ag-SP in the first step (Scheme 1b) and mixing with the selected nonionic surfactant (Scheme 1c) in the second step. In both methods, the presence of SP as the support allowed for the control of Ag size, which was dependent on the amount of SP present. The role of the nonionic surfactant poly(oxyethylene) C18-alkyl ether in the in situ process was to assist in the formation of tricomponent nanohybrids, Ag-SP-S, which are different from Ag-SP+S. Specifically, the poly(oxyethylene) segment in the surfactant molecules provides the chelating effect during $AgNO_3$ reduction to Ag nanoparticles because of the surfactant modification of the SP ionic character. It is noteworthy that the geometric shape of nanometer-thick SP has a lateral dimension of 80–100 nm in width and only 1 nm in thickness, providing a large surface area for interacting with the in situ generated Ag. The inherently high aggregation force among the nanoparticles by van der Waals attraction was overcome by the SP surface ionic interaction with individual Ag. The in situ generation of Ag in the presence of SP and surfactant to afford Ag-SP-S was compared to the physical blends of pregenerated Ag-SP and the same surfactant (Ag-SP+S), as shown in Scheme 1c. Various blending compositions with different surfactant content from 10 to 70 (weight ratio, %) were generated for comparison.

The X-ray diffraction (XRD) patterns illustrated that Ag was generated in high purity without the side reaction of forming silver oxides from air oxidation, as shown in Figure S1. The Ag-SP samples showed Ag-(111), Ag-(200), Ag-(220), and Ag-(311) diffraction peaks as the characterization of face-centered-cubic (fcc) alloy structure for metallic silver. The positions of the four peaks corresponding well to the JCPDS standard data for cubic-phase Ag (metallic Ag, JCPDS file: 65-2871). Furthermore, X-ray photoelectron spectroscopy (XPS) provides a sensitive measurement of the chemical state in the surface region of the silicates and Ag-silicate nanocomposites. In Figure 1a, high-resolution Si 2p spectra revealed information on the Ag–Si interaction, showing the binding energy between Ag and Si atoms in Ag-SP with an enormous shift of binding energy from 105.6 ($Si–O^-Na^+$, SP, black line) to 102.6 eV ($Si–O–Ag^+$, Ag-SP, green line), implying the existence of interaction forces between Ag and the silicate surface. A slight shift of the binding energy from 105.6 (SP, black line) to 105.2 eV (SP-S, red line) was noticed, presumably because of the chelation between poly(oxyethylene) or $(-CH_2CH_2O)_x-$ segment in the surfactant and sodium ions on the SP surface. The presence of surfactant caused a difference in the Ag interaction with SP, resulting in a binding-energy shift from 102.6 (Ag-SP, green line) to 101.9 eV (Ag-SP-S, blue line). In Figure 1b, the Ag–Si interaction was further verified for the high-resolution oxygen O 1s spectra, showing the shift from 534.6 (SP, black line) to 532.1 eV (Ag-SP, green line) and indicating a considerably strong interaction between the Ag and silicate anion. It is noted that the chemical shifts for Ag-SP-S and Ag-SP+S are significantly different, with the chemical shift occuring from Ag-SP (532.1 eV, green line) to Ag-SP-S (531.1 eV, blue line) versus no shift for Ag-SP and Ag-SP+S for the physically added surfactant. This is the direct evidence for the interaction of the surfactant in Ag-SP-S by the in situ synthesis.

Table 1. Correlation of SERS Intensity, Surfactant Fraction, and Silver Particle Size in Ag-SP-S Tricomponent Nanohybrids

		30/70/X				
weight fractions of Ag-SP-S fraction X (surfactant)[a]		0	8	17	35	70
mean diameter (nm)[b]		17.0 ± 5.0	14.3 ± 5.5	12.8 ± 3.5	11.8 ± 4.7	5.7 ± 3.1
SERS intensity × 10^{-3}[c]	*S. aureus*	139.1 ± 13.2	101.7 ± 8.7	88.0 ± 17.9	27.4 ± 7.6	10.4 ± 3.4
	E. coli	10.4 ± 4.3	26.7 ± 3.5	30.2 ± 4.4	32.0 ± 5.2	15.4 ± 3.8
		30/35/X				
weight fractions of Ag-SP-S fraction X (surfactant)[a]		0	8	17	35	70
mean diameter (nm)[b]		30.5 ± 20.3	23.1 ± 10.2	19.3 ± 7.4	18.4 ± 9.9	14.7 ± 5.9
SERS intensity × 10^{-3}[c]	*S. aureus*	218.3 ± 34.9	124.2 ± 7.6	115.0 ± 11.4	95.3 ± 14.4	84.7 ± 18.4
	E. coli	18.5 ± 5.2	69.7 ± 10.3	181.8 ± 16.4	110.3 ± 16.2	97.5 ± 20.0

[a]Weight fractions of Ag-SP-S. [b]Measured by TEM. [c]SERS intensity: integrated area of SERS peaks in the range from 700 and 770 cm^{-1}.

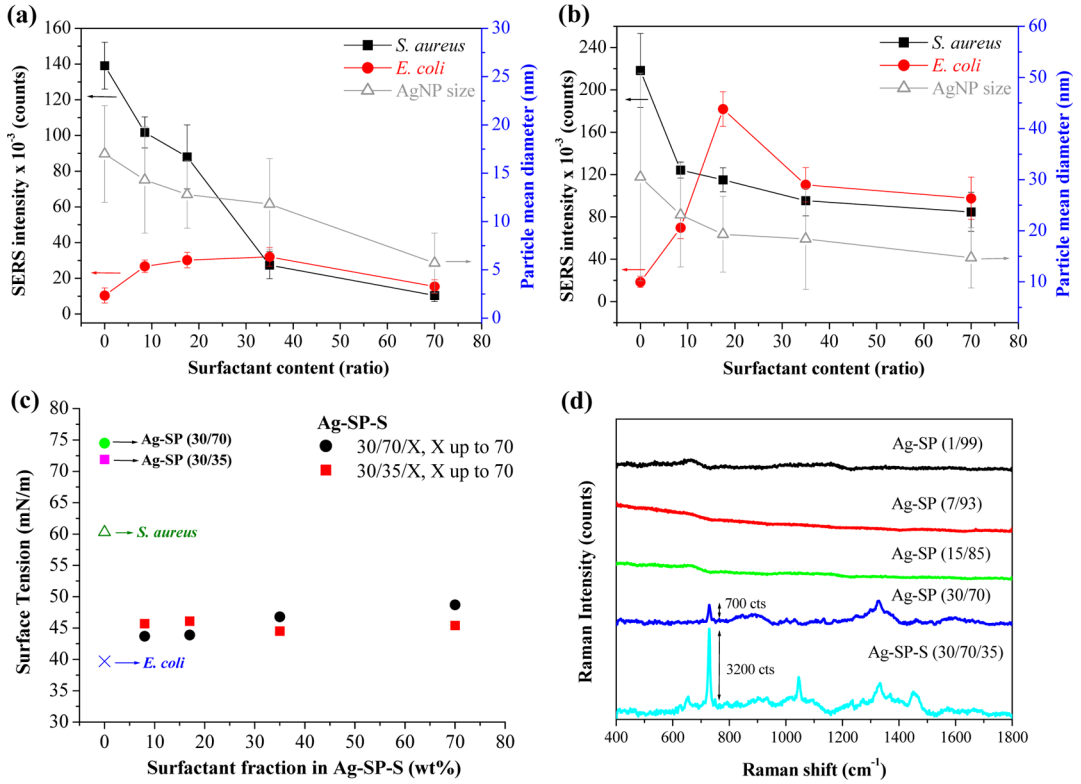

Figure 2. Correlation of SERS intensity and surfactant fraction in Ag-SP-S floating substrates for *S. aureus* (curve black square) and *E. coli* (curve red circle). Ag-SP-S at composition weight ratios of (a) 30/70/X, X = surfactant fraction from 0 to 70 and (b) 30/35/X, X = surfactant fraction from 0 to 70. Integration of SERS peak area between 700 and 770 cm^{-1} (gray triangle; particle sizes of AgNP in Ag-SP-S were determined by TEM observation). (c) Water surface tension of two series of Ag-SP-S tricomponent nanohybrids with varied fractions of surfactant in their composition and *S. aureus*[48] and *E. coli*.[49] (d) SERS spectra of *E. coli* measured using Ag-SP with a composition ratio from 1/99 to 30/70 and the selected Ag-SP-S at 30/70/35.

The SERS intensity for detecting *S. aureus* (a hydrophilic bacterium) and *E. coli* (a hydrophobic bacterium) was found to be dependent on the surfactant content in the Ag-SP-S nanohybrids. The TEM micrographs (Figure 1c–l) showed a slight change in Ag particle size when increasing the surfactant composition in the Ag-SP-S tricomponent nanohybrids. For example, the increase of the surfactant fraction in Ag-SP-S from weight ratios of 0, 8, 17, 37, and 70 to the pristine 30/70 Ag/SP bicomponent hybrids could affect only the Ag particle size, which decreased from 17, 14, 12, 12, and 5.7 nm in diameter. A similar trend was observed for the 30/35 Ag-SP from the in situ synthesis as a result of adding different surfactant amounts, with the Ag size dropping in the range of 30, 23, 19, 18, and 14 nm, respectively (Table 1).

These size variations and their association with the thin platelets and surfactants were correlated to the SERS intensity using these nanohybrids as the floating substrate, as shown in Table 1 and Figure 2. In Figure 2a, for *S. aureus* (black line), the strongest SERS signal appeared at zero surfactant content (the pristine Ag-SP without surfactant addition), whereas the trend of the SERS intensity was inversely dependent on surfactant participation (the SERS spectra is shown in Figure S2a). It can be rationalized that the surfactant in Ag-SP-S may alter the interfacial interaction between the Ag-SP and the bacteria, which have a different surface affinity for organic surfactant. In the case of *S. aureus*, the poly(oxyethylene) segment tends to chelate onto SP, and the resultant hydrophobic alkyl tails have a poor affinity for the surface of the hydrophilic bacterial cell. The

dx.doi.org/10.1021/am404218u | ACS Appl. Mater. Interfaces 2014, 6, 1541–1549

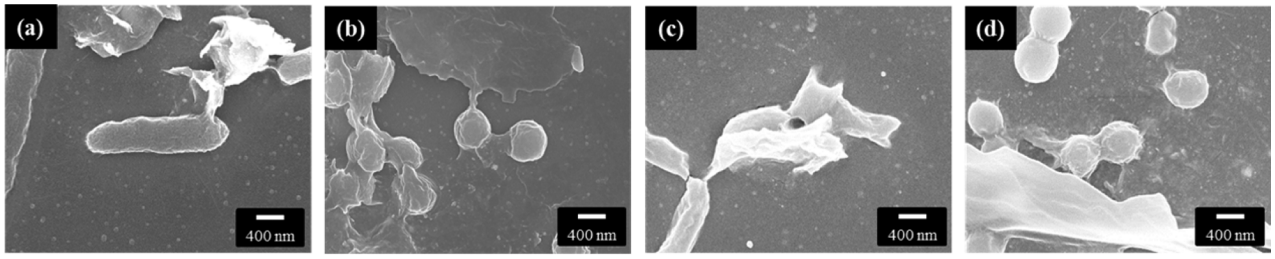

Figure 3. SEM images of actual contacts between SERS substrate and bacteria. (a) Ag-SP at a 30/70 weight ratio on *E. coli*, (b) Ag-SP at a 30/70 weight ratio on *S. aureus*, (c) Ag-SP-S at a 30/70/35 weight ratio on *E. coli*, and (d) Ag-SP-S at a 30/70/35 weight ratio on *S. aureus*.

Scheme 2. Mechanism of Ag-SP and Ag-SP-S Contact with Hydrophilic and Hydrophobic Microbes[a]

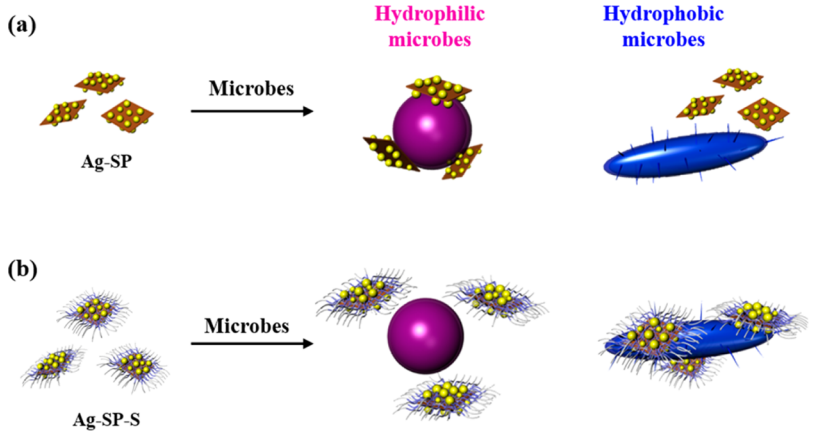

[a](a) Ag-SP and (b) Ag-SP-S.

presence of surfactant also slightly affected the Ag size, from 17.0 to 5.7 nm in diameter, although the Ag size became smaller by increasing the amount of surfactant in Ag-SP-S. When detecting *E. coli*, as indicated in Figure 2a, the SERS intensity (red line) in the range of 700−770 cm^{-1} was extremely low using the Ag-SP substrate; however, Ag-SP-S, with an increasing composition of surfactant, enhanced the SERS peaks with an optimized surfactant composition of 10−40 wt %. The optimal SERS intensity (34.9×10^3 counts) was 5-fold more than that using Ag-SP without surfactant (6.9×10^3 counts, SERS spectrum shown in Figure S2b)

Previous theoretical and experimental works indicated the possibility of controlling the size of Ag from 10 to 60 nm in diameter for SERS enhancement.[45,46] The control of particle size was achieved by the composition of the SP support[26] as well as the surfactant addition during the in situ reduction of $AgNO_3$. The enhancement of SERS sensitivity using Ag-SP-S as the floating substrate was found to be different for the varied bacterial species. Two series of Ag/SP weight ratios of 30/70 and 30/35 were investigated. In Figure 2b, the SERS intensity of *S. aureus* (black line) by Ag-SP 30/35 was increased nearly 2-fold more than by Ag-SP 30/70, but it decreased when the surfactant addition was involved (the SERS spectrum is in Figure S2c). In Figure 2b, the surfactant effect was found in detecting *E. coli*. With the increasing composition of surfactant, the SERS intensity (red line) was significantly enhanced and achieved an optimal value (181.8×10^3 counts) with a surfactant ratio in the range of 10−30 wt %. In summary, the Ag-SP 30/35 series displayed a 6-fold stronger signal for the optimal SERS intensity compared to the Ag-SP 30/70 series (34.9×10^3 counts; the SERS spectrum is shown in Figure S2d).

The interfacial interaction between the Ag nanohybrids and the bacteria surface could be one of the important factors for affecting SERS sensitivity. Because of the presence of lipopolysaccharide (LPS) on their outer membrane,[47] the *E. coli* cells displayed a hydrophobic property, as indicated by their surface free energy (γ) of 39.7 mJ/m^2.[48] The measurement for the pristine Ag-SP without surfactant modification was 75 mN/m (Figure 2c). The difference in the surface energy implies the degree of surface contact between Ag-SP and bacteria and consequently the Raman enhancement. In Figure 3b, four additional different compositions of Ag-SP and Ag sizes ranging from 3.8 nm in Ag/SP (1/99) to 17.0 nm in Ag/SP (30/70) are shown with their correlations for affinity for *E. coli*. All indicated no SERS enhancement. In contrast, surface free energy (γ) of *S. aureus* at pH 7 was shown to be 60.3 mJ/m^2,[49] which was relatively close to Ag-SP (75 mN/m). When surfactant was introduced, the surface free energy of Ag-SP-S significantly decreased from 75 to 45 mJ/m^2, which was close to that of *E. coli* (39.7 mJ/m^2). Apparently, the surfactant acts as an amphiphilic moiety to alter Ag-SP to be more hydrophobic in nature and hence higher in affinity for contacting the hydrophobic bacterial surface. In Figure 2d, a strong enhancement of *E. coli* on Ag-SP-S 30/70/35 (light blue line) can be seen, indicating the high interaction of Ag and the hydrophobic microbes. These values of the surface tension and energy of the nanohybrids toward bacteria are recorded in Table S1.

In Figure 3, SEM micrographs illustrate the actual contacts between the floating SERS substrates and bacteria. In the Ag-SP series (without surfactant), the interaction between hydrophilic Ag-SP and hydrophobic *E. coli* was relatively poor (Figure 3a), so the Ag-SP nanohybrids tended to self-aggregate and had less

contact with *E. coli*. By comparison, the same substrates had better contact with hydrophilic *S. aureus* (Figure 3b). In the Ag-SP-S series (with surfactant), good adhesion on the surface of *E. coli* (Figure 3c) was observed and rationalized by their similarities in surface energy. In contrast, the contact with *S. aureus* was relatively weak (Figure 3d) because of the difference in surface energy. The mechanism of Ag-SP and Ag-SP-S in contacting the bacterial surface can largely affect the sensitivity of SERS intensity, as shown in Scheme 2a,b, respectively. Ag-SP exhibited a stronger affinity for the hydrophilic microbe (*S. aureus*), whereas Ag-SP-S demonstrated better contact with the hydrophobic microbe (*E. coli*).

To understand the role of the surfactant in the tricomponent nanohybrids, the physical blends of Ag-SP and the surfactant (S) were investigated. Ag-SP (30/70 weight ratio and 17 nm Ag in diameter) was physically mixed with the surfactant in the amount of 10−70 wt %, which was analogous to the compositions of Ag-SP-S, to produce Ag-SP+S. As a result, the corresponding SERS intensity of *S. aureus* decreased from 137.0×10^3 to 3.5×10^3 counts by introducing the surfactant in the physical manner, as shown in Figure 4a (black line). However, the SERS intensity of *E. coli* remained almost the same or a slightly decreased from 10.4×10^3 to 1.0×10^3 (red line). In another series of Ag-SP at a 7/93 weight ration for Ag-SP+S (5 nm Ag in diameter), a lower SERS sensitivity (Figure 4b) for both *E. coli* (from 0.9×10^3 to 0.4×10^3) and *S. aureus* (from 54.3×10^3 to 0.5×10^3) was also demonstrated. The physically mixed Ag-SP+S showed significant differences from Ag-SP-S (generated by in situ synthesis), which demonstrated sufficient Raman enhancement. It was noted that the surfactant effect was more predominant than the Ag particle size. These results indicated the uniqueness of the tricomponent Ag-SP-S by in situ synthesis in comparison to the physically blended Ag-SP+S. The phenomenon was correlated to the binding energy difference at the molecular level (Figure 1). The binding energy of Ag-SP-S (in situ synthesis) exhibited a significant shift from analogous Ag-SP, whereas Ag-SP+S (physical blend) remained the same as Ag-SP in binding energy. The mutual interaction through the tricomponent hybridization of SP, surfactant, and Ag nanoparticles is crucial for the nanohybrids to interact with individual bacteria.

Because the development of a method for rapidly sensing mycobacteria is rather difficult as a result of the low growth rate and hydrophobic nature of the bacteria, the Ag-SP-S SERS substrate was tested for detecting the super-hydrophobic bacterium, *M. smegmatis*. The SERS signals using Ag-SP-S (30/35/X) with various surfactant compositions ranging from X = 8 to 70 are shown in Figure 5. The characteristic SERS peaks for the bacteria using Ag-SP-S appeared to have a Raman shift at 475 cm^{-1} and also in the range of 1300−1600 cm^{-1}, whereas 1046 cm^{-1} was the background signal of Ag-SP-S (blue line). In the Raman signal, *M. smegmatis* showed none of the characteristic peaks (orange line). The Ag-SP-S substrate has the potential for being developed into a sensor for detecting super-hydrophobic bacteria by adjusting the surfactant modification. The surfactant composition in the tricomponent Ag-SP-S could enhance the bacterial contact and display the characteristic detection for the specific bacteria.

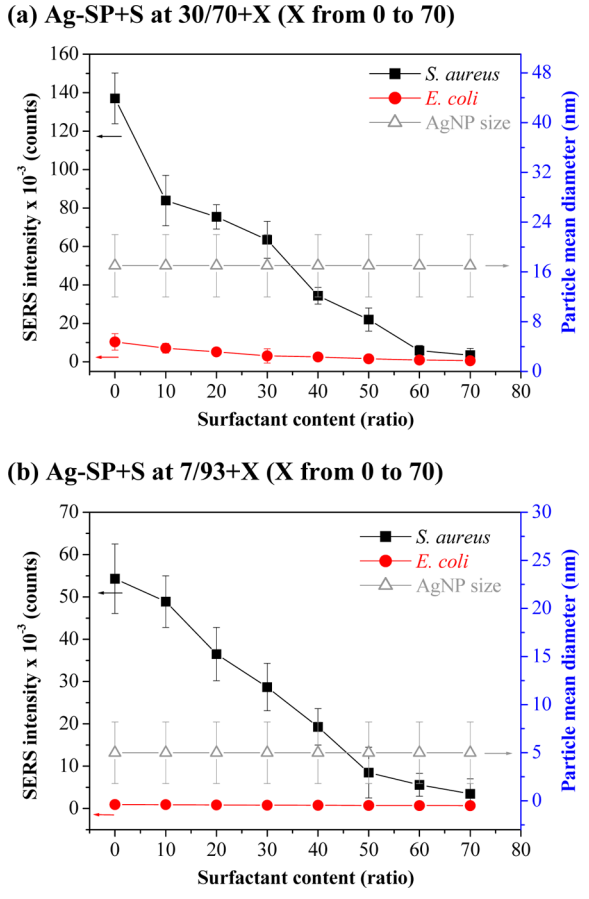

Figure 4. SERS intensity of *S. aureus* and *E. coli* detected by Ag-SP+S in various surfactant fractions synthesized by physical-blending. Ag-SP +S at composition weight ratios of (a) 30/70+X, X = surfactant fraction from 0 to 70 (the gray line shows the AgNP size of Ag-SP 30/70 at 17 nm) and (b) 7/93+X, X = surfactant fraction from 0 to 70 (the gray line shows the AgNP sizes of Ag-SP 7/93 at 5 nm). SERS intensity was integrated between 700 and 770 cm^{-1}.

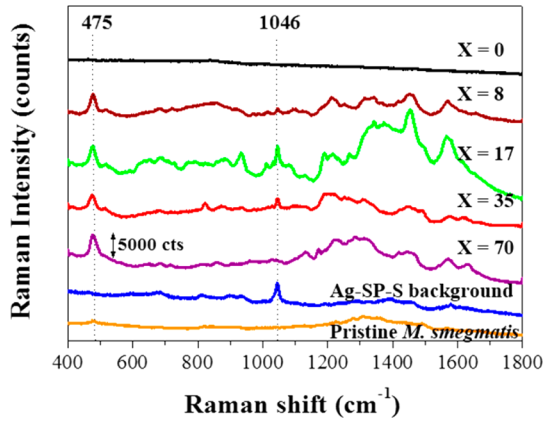

Figure 5. SERS spectra of *M. smegmatis* with various composition ratios of Ag-SP-S at 30/35/X, where X = surfactant fraction from 0 to 70.

4. CONCLUSIONS

We demonstrated a novel, flexible SERS substrate with 3D hot-junction capability as well as selective SERS detection for hydrophobic microorganisms by employing tricomponent nanohybrids of silver (Ag)-silicate platelet (SP)-surfactant (S). The selective SERS biodetection was emphasized, and the effect of the 3D hot junctions was discussed in the Supporting Information (Figure S3). The effective SERS

dx.doi.org/10.1021/am404218u | ACS Appl. Mater. Interfaces 2014, 6, 1541−1549

substrate, composed of Ag nanoparticles, nanosilicate platelets, and in situ added surfactant, was fabricated and compared with conventional SERS substrates of nanoparticles (<50 nm) on rigid (glass or silicon-based) substrates (1−10 cm).[50−52] The novel nanohybrid arrays of silver-on-silicate platelets (size: 100 nm to submicrometer) exhibited several advantages such the high flexibility, stability, and mobility of the substrate for contacting microorganisms as well as optical transparency for reducing the interfering background SERS signals, which can improve the stability of free nanoparticles and the mobility of rigid substrate in SERS detection technology. In particular, the surfactant modification allowed for the tailoring of the floating tricomponent nanohybrids to contact hydrophobic bacteria during SERS detection. The surface energy of the floating SERS substrates could be adjusted by changing the surfactant amount for selectively detecting hydrophilic or hydrophobic bacteria. Even for super-hydrophobic *M. smegmatis* detection, the Ag-SP-S displayed an effective and reproducible SERS spectrum in a fast mode. Comparable compositions were also produced by physical blending, resulting in Ag-SP+S, which failed to enhance the Raman signal. The findings of surfactant-modified Ag on silicate nanoplatelets may open new avenues for developing the ability to detect various types of pathogenic microorganisms selectively, including hydrophobic and irregular-shaped biological cells.

■ ASSOCIATED CONTENT

Supporting Information

Surface energy and interfacial affinity between Ag-SP-S and bacteria; wide-angle X-ray diffraction pattern of Ag-SP (30/70) and Ag-SP-S (30/70/70) for characterizing the formation of silver metal nanoparticles; SERS spectra of Ag-SP-S; and 3D hot-junctions capability of the Ag-SP SERS substrate. This material is available free of charge via the Internet at http://pubs.acs.org.

■ AUTHOR INFORMATION

Corresponding Authors

*E-mail: tyliu0322@gmail.com (T.-Y.L.).
*E-mail: jianglin@ntu.edu.tw (J.-J.L.).

Notes

The authors declare no competing financial interest.

■ ACKNOWLEDGMENTS

This work was financially supported by the National Science Council of Taiwan, the Ministry of Economics of Taiwan, and the Investigator Award of Academia Sinica. Technical support from the Core Facilities for Nanoscience and Nanotechnology at the Academia Sinica of Taiwan is acknowledged.

■ REFERENCES

(1) Tripp, R. A.; Dluhy, R. A.; Zhao, Y. *Nano Today* **2008**, *3*, 31−37.
(2) Moore, B. D.; Stevenson, L.; Watt, A.; Flitsch, S.; Turner, N. J.; Cassidy, C.; Graham, D. *Nat. Biotechnol.* **2004**, *22*, 1133−1138.
(3) Varnum, S. M.; Warner, M. G.; Dockendorff, B.; Anheier, N. C., Jr.; Lou, J.; Marks, J. D.; Smith, L. A.; Feldhaus, M. J.; Grate, J. W.; Bruckner-Lea, C. J. *Anal. Chim. Acta* **2006**, *570*, 137−143.
(4) Kempf, V. A. J.; Mändle, T.; Schumacher, U.; Schäfer, A.; Autenrieth, I. B. *Int. J. Med. Microbiol.* **2005**, *295*, 47−55.
(5) Park, C. H.; Vandel, N. M.; Hixon, D. L. *J. Clin. Microbiol.* **1996**, *34*, 988−990.
(6) Oberst, R. D.; Hays, M. P.; Bohra, L. K.; Phebus, R. K.; Yamashiro, C. T.; Paszko-Kolva, C.; Flood, S. J. A.; Sargeant, J. M.; Gillespie, J. R. *Appl. Environ. Microbiol.* **1998**, *64*, 3389−3396.
(7) Su, X. L.; Li, Y. *Biosens. Bioelectron.* **2004**, *19*, 563−574.
(8) Maalouf, R.; Fournier-Wirth, C.; Coste, J.; Chebib, H.; Saikali, Y.; Vittori, O.; Errachid, A.; Cloarec, J. P.; Martelet, C.; Jaffrezic-Renault, N. *Anal. Chem.* **2007**, *79*, 4879−4886.
(9) Casadio, F.; Leona, M.; Lombardi, J. R.; Van Duyne, R. *Acc. Chem. Res.* **2010**, *43*, 782−791.
(10) Nie, S.; Emory, S. R. *Science* **1997**, *275*, 1102−1106.
(11) Shachaf, C. M.; Elchuri, S. V.; Koh, A. L.; Zhu, J.; Nguyen, L. N.; Mitchell, D. J.; Zhang, J.; Swartz, K. B.; Sun, L.; Chan, S.; Sinclair, R.; Nolan, G. P. *PLoS One* **2009**, *4*, e5206-1−e5206-12.
(12) Qian, X.; Peng, X. H.; Ansari, D. O.; Yin-Goen, Q.; Chen, G. Z.; Shin, D. M.; Yang, L.; Young, A. N.; Wang, M. D.; Nie, S. *Nat. Biotechnol.* **2008**, *26*, 83−90.
(13) Jarvis, R. M.; Goodacre, R. *Chem. Soc. Rev.* **2008**, *37*, 931−936.
(14) Wang, H. H.; Liu, C. Y.; Wu, S. B.; Liu, N. W.; Peng, C. Y.; Chan, T. H.; Hsu, C. F.; Wang, J. K.; Wang, Y. L. *Adv. Mater.* **2006**, *18*, 491−495.
(15) Liu, T. T.; Lin, Y. H.; Hung, C. S.; Liu, T. J.; Chen, Y.; Huang, Y. C.; Tsai, T. H.; Wang, H. H.; Wang, D. W.; Wang, J. K.; Wang, Y. L.; Lin, C. H. *PLoS One* **2009**, *4*, e5470-1−e5470-10.
(16) Liu, T. Y.; Tsai, K. T.; Wang, H. H.; Chen, Y.; Chen, Y. H.; Chao, Y. C.; Chang, H. H.; Lin, C. H.; Wang, J. K.; Wang, Y. L. *Nat. Commun.* **2011**, *2*, 538−538.
(17) Liu, T. Y.; Chen, Y.; Wang, H. H.; Huang, Y. L.; Chao, Y. C.; Tsai, K. T.; Cheng, W. C.; Chuang, C. Y.; Tsai, Y. H.; Huang, C. Y.; Wang, D. W.; Lin, C. H.; Wang, J. K.; Wang, Y. L. *J. Nanosci. Nanotechnol.* **2012**, *12*, 5004−5008.
(18) Dong, R. X.; Chou, C. C.; Lin, J. J. *J. Mater. Chem.* **2009**, *19*, 2184−2188.
(19) Lin, J.-J.; Chu, C.-C.; Chou, C.-C.; Shieu, F.-S. *Adv. Mater.* **2005**, *17*, 301−304.
(20) Hsu, R. S.; Chang, W. H.; Lin, J. J. *ACS Appl. Mater. Interfaces* **2010**, *2*, 1349−1354.
(21) Su, H. L.; Chou, C. C.; Hung, D. J.; Lin, S. H.; Pao, I. C.; Lin, J. H.; Huang, F. L.; Dong, R. X.; Lin, J. J. *Biomaterials* **2009**, *30*, 5979−5987.
(22) Su, H. L.; Lin, S. H.; Wei, J. C.; Pao, I. C.; Chiao, S. H.; Huang, C. C.; Lin, S. Z.; Lin, J. J. *PLoS One* **2011**, *6*, e21125-1−e21125-10.
(23) Lin, J. J.; Lin, W. C.; Dong, R. X.; Hsu, S. H. *Nanotechnology* **2012**, *23*, 065102.
(24) Chiao, S. H.; Lin, S. H.; Shen, C. I.; Liao, J. W.; Bau, I. J.; Wei, J. C.; Tseng, L. P.; Hsu, S. H.; Lai, P. S.; Lin, S. Z.; Lin, J. J.; Su, H. L. *Int. J. Nanomed.* **2012**, *7*, 2421−2432.
(25) Lin, J. J.; Lin, W. C.; Li, S. D.; Lin, C. Y.; Hsu, S. H. *ACS Appl. Mater. Interfaces* **2013**, *5*, 433−443.
(26) Wei, J. C.; Yen, Y. T.; Wang, Y. T.; Hsu, S. H.; Lin, J. J. *RSC Adv.* **2013**, *3*, 7392−7397.
(27) Chu, C. Y.; Peng, F. C.; Chiu, Y. F.; Lee, H. C.; Chen, C. W.; Wei, J. C.; Lin, J. J. *PLoS One* **2012**, *7*, e38360-1−e38360-7.
(28) Wiley, B.; Sun, Y.; Xia, Y. *Acc. Chem. Res.* **2007**, *40*, 1067−1076.
(29) Rycenga, M.; Cobley, C. M.; Zeng, J.; Li, W.; Moran, C. H.; Zhang, Q.; Qin, D.; Xia, Y. *Chem. Rev.* **2011**, *111*, 3669−3712.
(30) Garcia-Vidal, F. J.; Pendry, J. B. *Phys. Rev. Lett.* **1996**, *77*, 1163−1166.
(31) Lu, L.; Eychmüller, A. *Acc. Chem. Res.* **2008**, *41*, 244−253.
(32) Lin, X. M.; Cui, Y.; Xu, Y. H.; Ren, B.; Tian, Z. Q. *Anal. Bioanal. Chem.* **2009**, *394*, 1729−1745.
(33) Tan, E. Z.; Yin, P. G.; You, T. T.; Wang, H.; Guo, L. *ACS Appl. Mater. Interfaces* **2012**, *4*, 3432−3437.
(34) Zhao, X.; Zhang, B.; Ai, K.; Zhang, G.; Cao, L.; Liu, X.; Sun, H.; Wang, H.; Lu, L. *J. Mater. Chem.* **2009**, *19*, 5547−5553.
(35) Yu, W. W.; White, I. M. *Anal. Chem.* **2010**, *82*, 9626−9630.
(36) Li, J.; Chen, L.; Lou, T.; Wang, Y. *ACS Appl. Mater. Interfaces* **2011**, *3*, 3936−3941.
(37) Anderson, D. J.; Moskovits, M. *J. Phys. Chem. B* **2006**, *110*, 13722−13727.

(38) Ren, W.; Fang, Y.; Wang, E. *ACS Nano* **2011**, *5*, 6425−6433.
(39) Song, J. E.; Phenrat, T.; Marinakos, S.; Xiao, Y.; Liu, J.; Wiesner, M. R.; Tilton, R. D.; Lowry, G. V. *Environ. Sci. Technol.* **2011**, *45*, 5988−5995.
(40) Wang, D. Y.; Teng, T. S.; Wu, Y. C.; Lee, Y. C.; Chen, K. H.; Chen, C. H.; Chang, Y. C.; Chen, C. C. *J. Phys. Chem. C* **2009**, *113*, 13498−13504.
(41) Jana, D.; Mandal, A.; De, G. *ACS Appl. Mater. Interfaces* **2012**, *4*, 3330−3334.
(42) Lin, J. J.; Chang, Y. C.; Cheng, I. *Macromol. Rapid Commun.* **2004**, *25*, 508−512.
(43) Chou, C. C.; Lin, J. J. *Macromolecules* **2005**, *38*, 230−233.
(44) Morhac, M.; Matousek, V. P. *Appl. Spectrosc.* **2008**, *62*, 91−106.
(45) Kelly, K. L.; Coronado, E.; Zhao, L. L.; Schatz, G. C. *J. Phys. Chem. B* **2002**, *107*, 668−677.
(46) Stamplecoskie, K. G.; Scaiano, J. C.; Tiwari, V. S.; Anis, H. *J. Phys. Chem. C* **2011**, *115*, 1403−1409.
(47) Dixon, D. R.; Darveau, R. P. *J. Dent. Res.* **2005**, *84*, 584−595.
(48) Khan, M. M.; Ista, L. K.; Lopez, G. P.; Schuler, A. J. *Environ. Sci. Technol.* **2011**, *45*, 1055−1060.
(49) Zmantar, T.; Bettaieb, F.; Chaieb, K.; Ezzili, B.; Mora-Ponsonnet, L.; Othmane, A.; Jaffrézic, N.; Bakhrouf, A. *World J. Microbiol. Biotechnol.* **2011**, *27*, 887−896.
(50) Zheng, W.; Chiamori, H. C.; Liu, G. L.; Lin, L.; Chen, F. F. *Nanotechnol. Rev.* **2012**, *1*, 213−233.
(51) Wu, X.; Xu, C.; Tripp, R. A.; Huang, Y.; Zhao, Y. *Analyst* **2013**, *138*, 3005−3012.
(52) Lu, Y.; Liu, G. L.; Lee, L. P. *Nano Lett.* **2005**, *5*, 5−9.